

# Topological insulators in ordered double transition metals $M_2M''C_2$ ( $M' = \text{Mo, W}$ ; $M'' = \text{Ti, Zr, Hf}$ ) MXenes

Mohammad Khazaei,<sup>1</sup> Ahmad Ranjbar,<sup>1</sup> Masao Arai,<sup>2</sup> and Seiji Yunoki<sup>1,3,4</sup>

<sup>1</sup>Computational Materials Science Research Team, RIKEN Advanced Institute for Computational Science (AICS), Kobe, Hyogo 650-0047, Japan

<sup>2</sup>International Center for Materials Nanoarchitectonics,

National Institute for Materials Science (NIMS), 1-1 Namiki, Tsukuba 305-0044, Ibaraki, Japan

<sup>3</sup>Computational Condensed Matter Physics Laboratory, RIKEN, Wako, Saitama 351-0198, Japan

<sup>4</sup>Computational Quantum Matter Research Team, RIKEN Center for Emergent Matter Science (CEMS), Wako, Saitama 351-0198, Japan

(Dated: October 4, 2016)

The family of two-dimensional transition metal carbides, so called MXenes, has recently found new members with ordered double transition metals  $M_2M''C_2$ , where  $M'$  and  $M''$  stand for transition metals. Here, using a set of first-principles calculations, we demonstrate that some of the newly added members, oxide  $M_2M''C_2$  ( $M' = \text{Mo, W}$ ;  $M'' = \text{Ti, Zr, Hf}$ ) MXenes, are topological insulators. The nontrivial topological states of the predicted MXenes are revealed by the  $Z_2$  index, which is evaluated from the parities of the occupied bands below the Fermi energy at time reversal invariant momenta, and also by the presence of the edge states. The predicted  $M_2M''C_2O_2$  MXenes show nontrivial gaps in the range of 0.041 – 0.285 eV within the generalized gradient approximation and 0.119 – 0.401 eV within the hybrid functional. The band gaps are induced by the spin-orbit coupling within the degenerate states with  $d_{x^2-y^2}$  and  $d_{xy}$  characters of  $M'$  and  $M''$ , while the band inversion occurs at the  $\Gamma$  point among the degenerate  $d_{x^2-y^2}/d_{xy}$  orbitals and a non-degenerate  $d_{3z^2-r^2}$  orbital, which is driven by the hybridization of the neighboring orbitals. The phonon dispersion calculations find that the predicted topological insulators are structurally stable. The predicted W-based MXenes with large band gaps might be suitable candidates for many topological applications at room temperature. In addition, we study the electronic structures of thicker ordered double transition metals  $M_2M'_2C_3O_2$  ( $M' = \text{Mo, W}$ ;  $M'' = \text{Ti, Zr, Hf}$ ) and find that they are nontrivial topological semimetals. Among the predicted topological insulators and topological semimetals,  $\text{Mo}_2\text{TiC}_2$  and  $\text{Mo}_2\text{Ti}_2\text{C}_3$  functionalized with mixture of F, O, and OH have already been synthesized, and therefore some of the topological materials proposed here can be experimentally accessed.

PACS numbers: 73.20.At, 71.20.-b, 71.70.Ej, 73.22.-f

## I. INTRODUCTION

Topological insulators (TIs) [1–4] promise an avenue to realize fascinating applications such as dissipationless transport, spintronics, optoelectronics, thermoelectronics, fault-tolerant quantum computing, and efficient power transition [5–14]. This is due to their unique surface states that are topologically protected and thus robust against non-magnetic impurities and disorders. The existence of these remarkable electronic states in TIs is attributed to the large spin-orbit coupling (SOC) of their heavy elements. TIs can have two- or three-dimensional structures. The two-dimensional (2D) TIs possess two wire-like metallic edge states in which electrons propagate with opposite spins [15–38]. The three-dimensional TIs have metallic surface states that usually form a single or an odd number of Dirac cones at or around the Fermi level [9, 13, 15].

Recently, 2D systems have received a lot of attentions because of their high tunability of charge, spin, and orbital states as well as electron confinement by surface functionalization and thickness control. Owing to the great advance in experimental techniques in recent years, the number of synthesized 2D systems has significantly increased [39]. Among the recent synthesized structures, 2D transition metal carbides and nitrides, so called MXenes, have attracted considerable attentions due to their high mechanical stability, various elemental compositional and surface functional possibilities, and flexible thickness controllability. MXenes are a new class of

2D transition metal carbides and nitrides with chemical formula of  $M_{n+1}X_n$  ( $M = \text{Sc, Ti, V, Cr, Zr, Nb, Mo, Hf, Ta}$ ;  $X = \text{C, N}$ ) with  $n = 1, 2, 3$  that have recently been synthesized through hydrofluoric etching [40, 41] of layered MAX phase compounds  $M_{n+1}AX_n$ , where  $A = \text{Al, Si, P, S, Ga, Ge, As, In, and Sn}$  [42, 43]. During the etching process, the A element is washed out from the MAX phase structure and simultaneously the surfaces of the resulting 2D systems are chemically saturated with mixture of F, O, and OH [40, 41, 44, 45]. These 2D systems have been named MXenes because they originate from the MAX phases by removing A elements and because they are structurally analogous to the graphene [40, 41]. The 2D MXenes such as  $\text{Ti}_2\text{C}$ ,  $\text{V}_2\text{C}$ ,  $\text{Nb}_2\text{C}$ ,  $\text{Ta}_2\text{C}$ ,  $\text{Mo}_2\text{C}$ ,  $\text{Ti}_3\text{C}_2$ ,  $\text{Nb}_4\text{C}_3$  have already been synthesized [40, 41, 46, 47]. MXenes are known to have or predicted to have electronic, magnetic, and energy harvesting applications [48–62].

Theoretically, it has been shown that some of the MXenes possess Dirac band dispersions crossing at the Fermi level, owing to the honeycomb like structure [63]. Therefore, they are highly suspected for being TIs if heavy transition metal elements are involved. Indeed, we have previously shown that among the members of functionalized  $M_2X$  MXenes,  $\text{Mo}_2\text{CO}_2$  and  $\text{W}_2\text{CO}_2$  are TIs [64]. The family of MXenes has lately been expanded to the ordered double transition metals carbides  $M_2M''C_2$  and  $M_2M'_2C_3$ , where  $M'$  and  $M''$  stands for transition metals [65–67]. This breakthrough experiment is a major success because previously the MXenes with different transition metals such as  $\text{TiNbC}$ ,  $(\text{Ti}_{0.5}\text{V}_{0.5})_2\text{C}$ ,

( $V_{0.5}Cr_{0.5}$ ) $_3C_2$ ,  $Ti_3CN$ , and ( $Nb_{0.8}Ti_{0.2}$ ) $_4C$  could only be synthesized in the alloy forms [40, 41, 68, 69], but not the ordered ones. Here, using first-principles electronic structure calculations, we demonstrate that in this newly discovered MXenes, oxide  $M'_2M''C_2$  ( $M' = Mo, W; M'' = Ti, Zr, Hf$ ) are TIs with band gaps as large as 0.285 eV within the generalized gradient approximation 0.401 eV within the hybrid functional) and oxide  $M'_2M''_2C_3$  are nontrivial topological semimetals. Because  $Mo_2TiC_2$  and  $Mo_2Ti_2C_3$  MXenes with mixture of F, OH, and O surface chemical groups has already been synthesized [65, 66], some of the proposed oxide  $M'_2M''C_2$  and  $M'_2M''_2C_3$  will be experimentally accessed in the near future.

## II. METHOD OF CALCULATIONS

The structural optimizations and electronic structure calculations are performed in the context of density functional theory as implemented in VASP code [70]. Exchange-correlation energies are taken into account by the generalized gradient approximation (GGA) using Perdew-Burke-Ernzerhof functional [71]. The wave functions are constructed using projected augmented wave approach with plane wave cutoff energy of 520 eV. The effect of spin-orbit coupling (SOC) is included self-consistently in the electronic structure calculations. The atomic positions and cell parameters are fully optimized using conjugate gradient method without imposing any symmetry. After the optimization process, the maximum residual force on each atom is less than 0.001 eV/Å. The total energies are converged within  $10^{-6}$  eV/cell. A large vacuum space of 50 Å is set along the  $c$  axis, the direction perpendicular to the surface, to avoid any interaction between the layer and its periodic images. The Brillouin zone integration is sampled using a set of  $12 \times 12 \times 1$  Monkhorst-Pack  $\mathbf{k}$  points [72]. Since the GGA often underestimates the band gap, we also perform the hybrid functional [Heyd-Scuseria-Ernzerhof (HSE06)] calculations [73, 74] with 20  $\mathbf{k}$  points along each path section to check the band topology.

The phonon dispersions are obtained using the density functional perturbation theory in the same level of approximation as described above using Quantum Espresso code [75, 76]. The edge states are calculated using a nonuniform tight-binding Green's function method with maximally localized Wannier function basis sets [77, 78] generated by OpenMX code [79].

## III. RESULTS AND DISCUSSION

### A. Atomic structure

As shown in Fig. 1(a),  $M'_2M''C_2$  forms a hexagonal lattice with  $P\bar{3}m1$  group symmetry and is made of five atomic layers of  $M'-C-M''-C-M'$  where  $M'$  transition metals form the outer surfaces and  $M''$  transition metals form the central layer. The carbon atoms are sandwiched between the  $M'$  and  $M''$  transition metal layers, and each carbon atom is located at the center of an octahedral cage formed by  $M'$  and  $M''$  transition metals.

Theoretically, it has been shown that the ordered double transition metals MXenes is structurally stable, and indeed one of them,  $Mo_2TiC_2$ , has already been synthesized experimentally [65, 66].

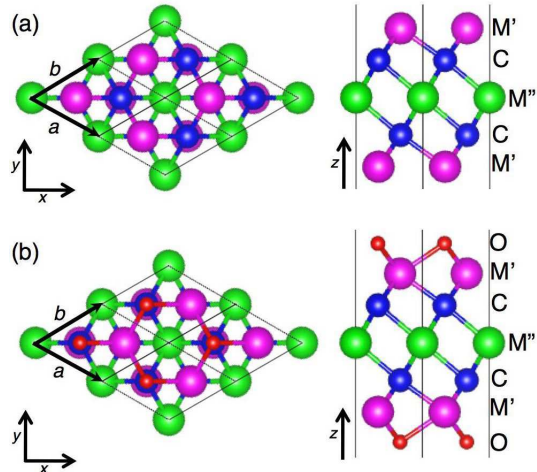


FIG. 1. (Color online) Top (left panels) and side (right panels) views of two-dimensional (a)  $M'_2M''C_2$  and (b)  $M'_2M''C_2O_2$  MXenes. The unit vectors in  $ab$  plane are denoted by black arrows.

It is very difficult to synthesize MXenes with pure surfaces from MAX phases by the etching process and usually the surfaces of MXenes are saturated with the mixture of chemical groups that depend on the type of applied chemical solution. For instance, when hydrofluoric acid is used, the surfaces of MXenes are saturated with the mixture of F, O, and OH [40, 41]. This is due to the high chemical reactivity of transition metals on the exposed surfaces of MXenes. It has been shown theoretically that the chemical groups such as F, O, and OH form strong bonding with the transition metals and thus the surfaces of MXenes can be fully saturated with them at a proper chemical potential [48, 80]. Pristine  $M'_2M''C_2$  ( $M' = Mo, W; M'' = Ti, Zr, Hf$ ) MXenes are metallic [65]. However, upon proper surface functionalization, some of the MXenes become semiconducting [48, 66]. Here, we shall focus on  $M'_2M''C_2$  ( $M' = Mo, W; M'' = Ti, Zr, Hf$ ) MXenes functionalized with oxygen to investigate the electronic properties in detail. Before studying the electronic structures, the structural properties of  $M'_2M''C_2O_2$  are examined.

Two oxygen atoms per unit cell are required to fully functionalize the surfaces of MXenes. Generally, the functional groups can be adsorbed on top of the transition metals or on top of hollow sites of the surfaces. However, the previous calculations find that the configurations with chemical groups adsorbed on top of the transition metals sites are energetically unfavorable and these chemical groups eventually move to top of the hollow sites after the structural optimization [48, 50]. Therefore, the chemical groups are favorably adsorbed on top of the hollow sites formed by the surface transition metals.

The surfaces of MXenes include two types of hollow sites, which are named as A and B here. At the B-type (A-type) hollow site, there is (is not) a carbon atom under the hollow.

TABLE I. The total energy (in eV) per unit cell of the optimized AA, AB, and BB models for  $M'_2M''C_2O_2$  ( $M' = \text{Mo, W}$ ;  $M'' = \text{Ti, Zr, Hf}$ ).

	AA	AB	BB
$\text{Mo}_2\text{TiC}_2\text{O}_2$	-64.057	-64.628	-65.238
$\text{Mo}_2\text{ZrC}_2\text{O}_2$	-64.436	-64.868	-65.388
$\text{Mo}_2\text{HfC}_2\text{O}_2$	-66.278	-66.765	-67.328
$\text{W}_2\text{TiC}_2\text{O}_2$	-68.336	-68.911	-69.588
$\text{W}_2\text{ZrC}_2\text{O}_2$	-68.769	-69.187	-69.747
$\text{W}_2\text{HfC}_2\text{O}_2$	-70.571	-71.075	-71.694

Therefore, depending on the relative positions of the attached oxygen groups at the hollow sites of the two surfaces, three different model configurations are possible for the chemical terminations of  $M'_2M''C_2$ : AA, AB, and BB models. In AA (BB) model, the two oxygen atoms are adsorbed on top of the A-type (B-type) hollow sites, while in AB model, one of the oxygen atoms is adsorbed on top of the A-type hollow site and the other one is adsorbed on top of the B-type hollow.

In order to find the most stable model structures, we fully optimized the structures of the above three models for each  $M'_2M''C_2O_2$  system. The total energies of the optimized models are summarized in Table I. Since the total energy is lowest for the BB systems, the BB model is considered to be the most appropriate for the  $M'_2M''C_2O_2$  ( $M' = \text{Mo, W}$ ;  $M'' = \text{Ti, Zr, Hf}$ ) MXenes. The most stable BB type structure for the  $M'_2M''C_2O_2$  MXenes is shown in Fig. 1(b) and the detailed crystal parameters are found in Supplemental Material [81].

In order to ensure that all atoms in the predicted  $M'_2M''C_2O_2$  structures are in their equilibrium positions, we also calculated a set of phonon dispersions. Typical examples of the phonon dispersions for  $\text{Mo}_2\text{TiC}_2\text{O}_2$  and  $\text{W}_2\text{HfC}_2\text{O}_2$  are shown in Fig. 2, the results for others are included into Supplemental Material [81]. As shown in Fig. 2, we find that all phonon modes are positive, indicating that the predicted structures are dynamically stable. The highest phonon frequency in  $M'_2M''C_2O_2$  MXenes is around  $780 \text{ cm}^{-1}$ , which is higher than that for  $\text{MoS}_2$   $475 \text{ cm}^{-1}$  [82], but lower than that for graphene  $1600 \text{ cm}^{-1}$  [83]. This indicates the  $M'_2M''C_2O_2$  MXenes have higher (lower) stability than  $\text{MoS}_2$  (graphene). The electronic structure analyses given in the following are based on the most stable structures obtained here in this section.

## B. Electronic structure

Since the band structures are qualitatively the same among all the  $M'_2M''C_2O_2$  MXenes studied here, we show in Fig. 3 the results for  $\text{W}_2\text{HfC}_2\text{O}_2$  with and without the SOC. The band structures for other MXenes are given in Supplemental Material [81]. As shown in Fig. 3, when the SOC is not considered, the system is semimetallic because the topmost valence band and the lowest conduction band touch only at the  $\Gamma$  point, around which the valence and conduction bands are both parabolic. In order to better analyze the band structures,

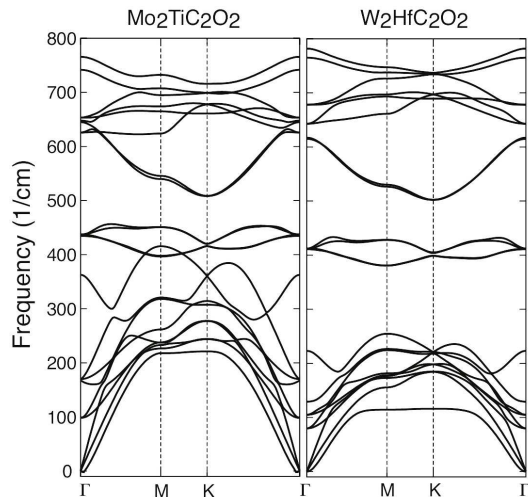


FIG. 2. Phonon dispersions for  $\text{Mo}_2\text{TiC}_2\text{O}_2$  and  $\text{W}_2\text{HfC}_2\text{O}_2$ .

the projected band structures onto each constituent element with different orbital symmetries are also shown in Fig. 3. We can easily find in Fig. 3 that the bands near the Fermi energy originates from  $d$  orbitals of transition metals  $M'$  and  $M''$ . Because of the hexagonal symmetry of the crystal structure, the  $d$  orbitals are categorized into three groups,  $(d_{xy}, d_{x^2-y^2})$ ,  $(d_{xz}, d_{yz})$ , and  $d_{3z^2-r^2}$ , although the former two groups belong to the same irreducible representation for  $D_{3d}$  symmetry. Similarly, the  $p$  orbitals are divided into two groups,  $(p_x, p_y)$  and  $p_z$ . As shown in Fig. 3, indeed, the topmost valence band and the lowest conduction band at the  $\Gamma$  point around the Fermi energy are dominated by  $d_{xy}$  and  $d_{x^2-y^2}$  orbitals of transition metals  $M'$  and  $M''$ .

Often, 2D materials composed of heavy elements with touching the valence and conduction bands at the Fermi energy are suspected for being TIs. This motivates us to examine the possible nontrivial band topology of  $M'_2M''C_2O_2$  MXenes. As shown in Fig. 3, upon considering the SOC, the degeneracy of the topmost valence band and the lowest conduction band at the Fermi energy is lifted (except for the Kramers degeneracy) and the band gap is open. Consequently, the  $M'_2M''C_2O_2$  MXenes ( $M' = \text{Mo, W}$ ;  $M'' = \text{Ti, Zr, Hf}$ ) turn into semiconductor with indirect band gaps, as summarized in Table II. It is clearly observed in Table II that the induced band gap is larger as the SOC (i.e., mass) of  $M'$  and/or  $M''$  is larger. We find that the band gap can be as large (small) as 0.285 eV (0.041 eV) for  $\text{W}_2\text{HfC}_2\text{O}_2$  ( $\text{Mo}_2\text{TiC}_2\text{O}_2$ ).

We further explore the effect of SOC on the band gap by turning on the SOC for a particular element, either  $M'$  or  $M''$  in  $M'_2M''C_2O_2$ . This can be done using Quantum Espresso [75, 76]. As expected, the results of the band gaps calculated using VASP and Quantum Espresso are almost the same when the SOC is on for all the elements (see Table II). When the SOC is switched on only for  $M'$  or  $M''$  element, the degeneracy of the topmost valence band and the lowest conduction band at the  $\Gamma$  point is lifted and the band gap is open, as summarized in Table II (and also see Supplemental

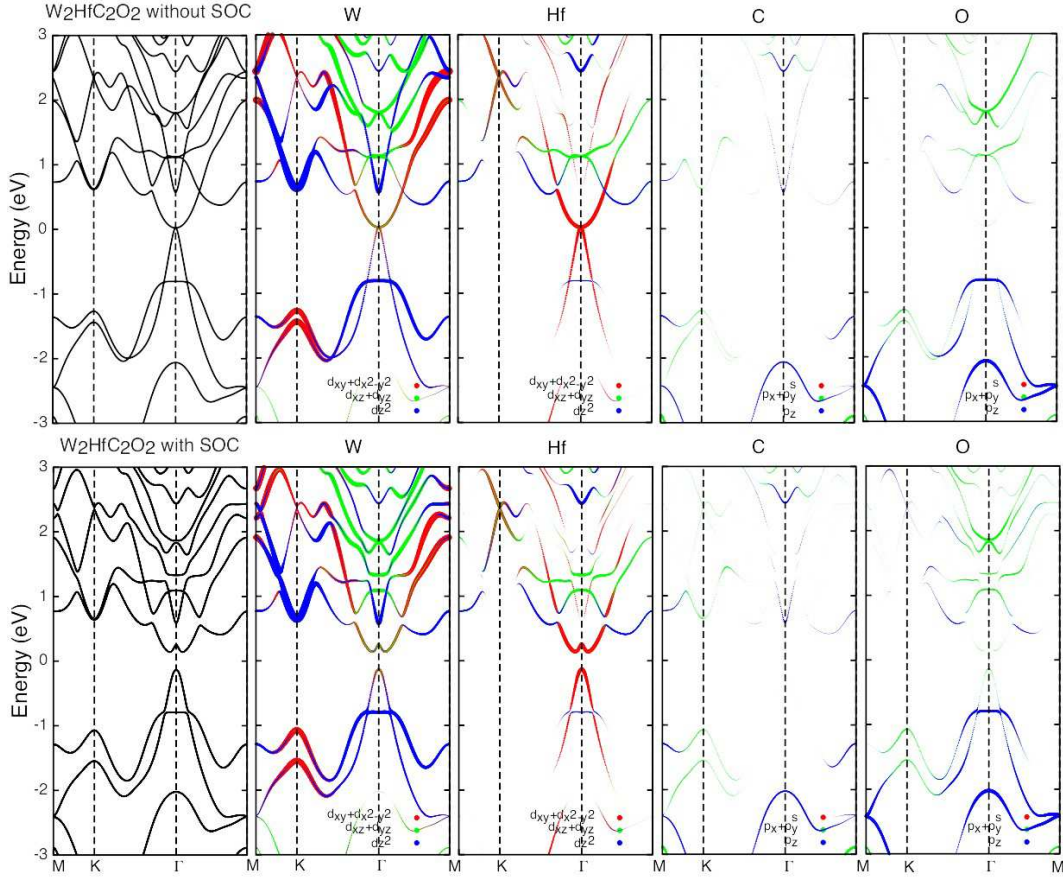


FIG. 3. (Color online) Electronic band structures for  $W_2HfC_2O_2$  without (top panels) and with the SOC (bottom panels). For detailed analysis, the band structures projected onto each constituent element with different orbital symmetries (indicated in the figures) are also shown. The Fermi energy is located at zero energy.

Material [81]), for all the  $M'_2M''C_2O_2$  MXenes studied here, implying that the strength of the SOC for either  $M'$  or  $M''$  is enough to open a gap in these systems. The degeneracy at the  $\Gamma$  point should be lifted because there is no four-dimensional irreducible representation for  $D_{3d}$  double group. However, notice that these band gaps are always smaller than those evaluated with the SOC on for both  $M'$  and  $M''$  elements. Comparing the band gaps for the different systems in Table II, we find that the SOC for each transition metal seems to contribute separately to opening the gap as large as  $\sim 0.026$ ,  $\sim 0.123$ ,  $\sim 0.01$ ,  $\sim 0.04$ , and  $\sim 0.14$  eV for Mo, W, Ti, Zr, and Hf, respectively. It is well known that the GGA calculations underestimate the band gaps. Hence, in order to better estimate the band gap as well as the band topology, we examine the band structures using the hybrid functionals (HSE06). As shown in the Supplemental Material [81], the similar band topologies are found through the hybrid calculations and the band gaps are estimated to be in the range of 0.119 – 0.401 eV (see Table II). To ensure that these insulators are topologically nontrivial, next we shall calculate the  $Z_2$  topological invariant.

Since all the  $M'_2M''C_2O_2$  MXenes studied here have the inversion symmetry, their  $Z_2$  topological invariant can be simply

calculated from the parity of their valence band wave functions at the time reversal invariant momentum (TRIM) points of the Brillouin zone [84, 85]. More precisely, the  $Z_2$  index  $\nu$  is evaluated as  $(-1)^\nu = \prod_{i=1}^4 \delta(k_i)$ , where  $\delta(k_i) = \prod_{n=1}^N \zeta_n^i$ ,  $\zeta_n^i (= \pm 1)$  is the parity of the  $n$ th valence band at the  $i$ th TRIM  $k_i$ , and  $N$  is the total number of the occupied valence bands [84, 85]. The trivial and nontrivial topological phases are characterized by  $\nu = 0$  and 1, respectively. Because the crystal structure of the  $M'_2M''C_2O_2$  MXenes is hexagonal (see Fig. 1), the TRIM points are at  $\Gamma$  point:  $\mathbf{k} = (0, 0)$ ,  $M_1$  point:  $\mathbf{k} = (0, 0.5)$ ,  $M_2$  point:  $\mathbf{k} = (0.5, 0)$ , and  $M_3$  point:  $\mathbf{k} = (0.5, 0.5)$ . Because of the hexagonal symmetry, the parities at the  $M_1$ ,  $M_2$ , and  $M_3$  points become equivalent, and commonly are identified as  $M$ . Thus the  $Z_2$  index can be simply obtained from  $(-1)^\nu = \delta^3(M)\delta(\Gamma)$ . From the parity analysis of the occupied bands at the TRIM points, we find that  $\nu = 1$  for all the systems studied here and therefore  $M'_2M''C_2O_2$  ( $M' = \text{Mo, W}$ ;  $M'' = \text{Ti, Zr, Hf}$ ) MXenes are TIs.

One of the remarkable characteristics of the TI is the presence of an odd number of topologically protected conducting edge states that cross the Fermi energy. In order to fur-

TABLE II. Band gaps (in eV) for  $M'_2M''C_2O_2$  ( $M' = \text{Mo}, \text{W}; M'' = \text{Ti}, \text{Zr}, \text{Hf}$ ) obtained using VASP and Quantum Espresso (QE) with the SOC on for all elements (second column). The results with the SOC on only for  $M'$  ( $M''$ ) element are also provided in the third (fourth) column, obtained using Quantum Espresso. The band gaps in the second, third, and fourth columns are obtained by the GGA. For comparison, band gaps obtained by the hybrid functional (HSE06) calculations using VASP are also provided in the fifth column.

	SOC is on for all elements (VASP/QE)	SOC is on for only $M'$	SOC is on for only $M''$	SOC is on for all elements with HSE06
$\text{Mo}_2\text{TiC}_2\text{O}_2$	0.041/0.036	0.027	0.009	0.119
$\text{Mo}_2\text{ZrC}_2\text{O}_2$	0.069/0.065	0.026	0.039	0.125
$\text{Mo}_2\text{HfC}_2\text{O}_2$	0.153/0.151	0.027	0.120	0.238
$\text{W}_2\text{TiC}_2\text{O}_2$	0.136/0.135	0.121	0.010	0.290
$\text{W}_2\text{ZrC}_2\text{O}_2$	0.170/0.166	0.123	0.040	0.280
$\text{W}_2\text{HfC}_2\text{O}_2$	0.285/0.285	0.135	0.140	0.409

ther confirm the nontrivial band topology, we also calculate the electronic band structures for the nanoribbon structures of  $\text{Mo}_2\text{TiC}_2\text{O}_2$  and  $\text{W}_2\text{HfC}_2\text{O}_2$  with symmetric edges by using the effective tight binding Hamiltonian, which are constructed based on the maximally localized Wannier functions. Since the electronic bands near the Fermi energy are mainly composed of  $d_{x^2-y^2}$ ,  $d_{xy}$ , and  $d_{3z^2-r^2}$  orbitals of transition metals  $M'$  and  $M''$  (see Fig. 3), the minimal tight binding Hamiltonian can be constructed using these orbitals. Figure 4 shows the results of the electronic band structures, which clearly displays that the edge bands cross the Fermi energy three times along the  $\bar{\Gamma}$ - $\bar{M}$  points for both systems.

### C. Discussion

Let us finally examine the origin of the topological insulating behavior found in the  $M'_2M''C_2O_2$  MXenes. As shown in Fig. 3, the SOC is essential to open a finite band gap but does not induce the band inversion that is necessary to change the band topology, implying that the band inversion has already occurred in the  $M'_2M''C_2O_2$  MXenes before introducing the SOC. This is thus different from most of topological insulators for which the SOC is required to induce the band inversion [9–11, 18, 26], although some exceptions have been reported [16, 23, 27, 64].

To understand the band structures in more details, we investigate the evolution of the band structures without the SOC as the lattice constant is uniformly expanded from the optimized one that is obtained in Sec. III A. Note that the structure is not optimized when the lattice constant is expanded because this is much easier to analyze the evolution of the band structures. As shown in Fig. 5, the band structures around the Fermi energy are qualitatively the same until the lattice constant is expanded slightly below 20% ( $1.2a_0$ ), where the topmost valence band and the lowest conduction band remain touched (i.e., degenerate) at the  $\Gamma$  point and they are essentially com-

posed of  $d_{xy}$  and  $d_{x^2-y^2}$  orbitals of W and Hf. However, when the lattice constant is expanded more than  $\sim 20\%$ , the band gap opens and the band characters around the Fermi energy change qualitatively at the  $\Gamma$  point, where the topmost valence band is composed of  $d_{3z^2-r^2}$  orbital, while the lowest conduction bands are doubly degenerate and consist of  $d_{xy}$  and  $d_{x^2-y^2}$  orbitals. More interestingly, we find that the band inversion occurs at the  $\Gamma$  point concomitantly when the band gap opens. We should note that neither the band inversion nor the gap closing occurs at other momenta except for the  $\Gamma$  point.

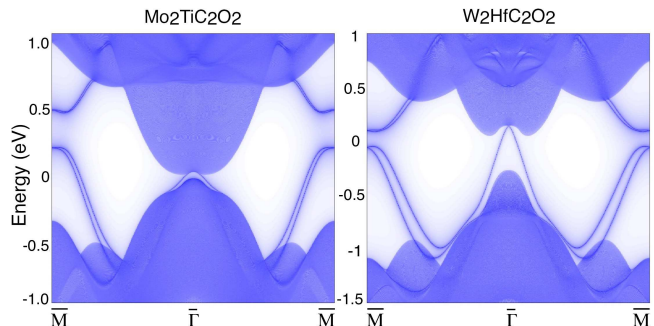


FIG. 4. (Color online) Edge band structures for  $\text{Mo}_2\text{TiC}_2\text{O}_2$  and  $\text{W}_2\text{HfC}_2\text{O}_2$ . The Fermi energy is located at zero energy.

The evolution of the electronic bands at the  $\Gamma$  point is summarized schematically in Fig. 6. When the lattice constant is very large ( $\geq 1.2a_0$ , where  $a_0$  is the optimized lattice constant in Sec. III A) and the SOC is absent,  $\text{W}_2\text{HfC}_2\text{O}_2$  is a trivial band insulator in which the two topmost valence bands are made of bonding and non-bonding states of  $d_{3z^2-r^2}$  orbitals with even and odd parities, respectively, while the lowest conduction bands are doubly degenerate and formed by a bonding state of  $d_{xy}/d_{x^2-y^2}$  orbitals with even parity. As the lattice constant is reduced, the hybridization between neighboring  $d$  orbitals increases. As a result, the bonding state of doubly degenerate  $d_{xy}/d_{x^2-y^2}$  orbitals shift downward below the Fermi energy, while the non-bonding state of  $d_{3z^2-r^2}$  orbital moves above the Fermi energy. Since these two states have opposite parities, this is precisely when the band inversion occurs. Note that the Fermi energy remains exactly at the doubly degenerate  $d_{xy}/d_{x^2-y^2}$  states once the band inversion occurs, and therefore the system remains semi-metallic. However, as soon as the SOC is introduced, the doubly degeneracy is lifted and the system becomes a nontrivial insulator. The role of the SOC is thus to induce a finite band gap but not a band inversion, which has similarly been observed in  $\text{ZrTe}_5$  [86], square-octagonal  $\text{WS}_2$  [15], MX ( $M=\text{Zr}, \text{Hf}; X=\text{Cl}, \text{Br}, \text{I}$ ) [16], and  $\text{W}_2\text{CO}_2$  systems [64].

It is worth summarizing the differences and similarities between the current study with our previous study in Ref. [64].  $\text{Mo}_2\text{CO}_2$  and  $\text{W}_2\text{CO}_2$  studied in Ref. [64] belong to the family of functionalized  $M_2X$  MXenes with two transition metal layers, while the systems studied here such as  $\text{Mo}_2\text{TiC}_2$  and  $\text{Mo}_2\text{ZrC}_2$  belong to the family of ordered double transition metal carbides  $M'_2M''C_2$  MXenes with three transition metal layers. For  $\text{Mo}_2\text{CO}_2$  and  $\text{W}_2\text{CO}_2$  as well as  $M'_2M''C_2O_2$  ( $M' =$

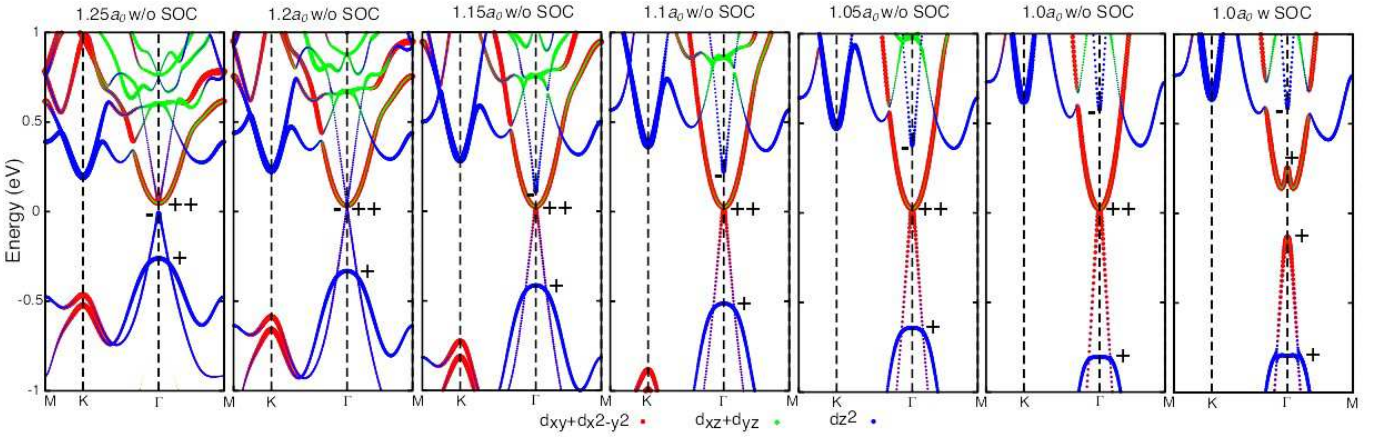


FIG. 5. (Color online) Band structure evolution of  $W_2HfC_2O_2$  projected onto  $d$  orbitals of W and Hf atoms as the lattice constant is expanded uniformly from the optimized one ( $a_0$ ) without (w/o) including the SOC. For comparison, the results for the optimized structure with the SOC is also shown. Fermi energy is at zero.

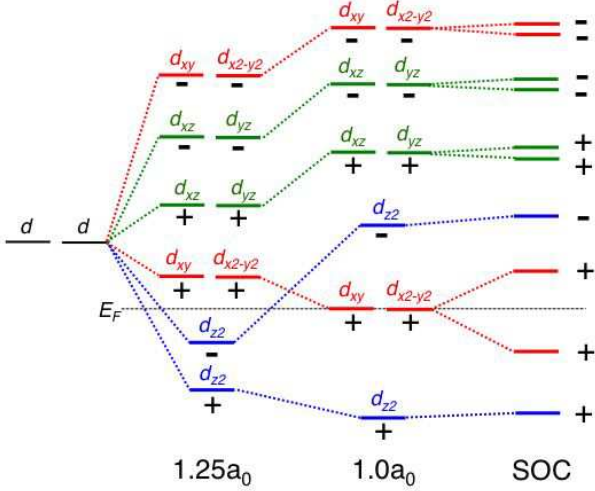


FIG. 6. (Color online) A schematically illustration of the evolution of the electronic bands at the  $\Gamma$  point as the lattice constant is uniformly decreased to the optimized one  $a_0$  without the SOC. The SOC is incorporated only in the left most figure. The bands are mainly drawn for W  $d$  orbitals, which have the highest contribution near the Fermi states. W  $d$ -orbitals are split by crystal fields, chemical bondings, and SOC.  $a_0$  is the optimized lattice constant and  $E_f$  is the Fermi energy.

Mo, W;  $M'' = Ti, Zr, Hf$ ), the SOC is essential to open a finite band gap, but does not induce the band inversion. The mechanism of the band inversion in  $M'_2M''C_2O_2$  MXenes described above is similar to that in  $Mo_2CO_2$  and  $W_2CO_2$ . The resulting topological band gap in the  $M'_2M''C_2$  MXenes can be as large as that in  $W_2CO_2$  (0.19 eV within the GGA and 0.47 eV within the hybrid functional).

We have also studied the electronic structures of  $M'_2M''C_3O_2$  ( $M' = Mo, W; M'' = Ti, Zr, Hf$ ), i.e., MXenes with four transition metal layers. Similar to the  $M'_2M''C_2O_2$

systems, they have hexagonal structures with  $P\bar{3}m1$  space group symmetry and the BB model represents the most stable atomic configuration. The total energies, crystal structures, and band structures without and with the SOC are shown in Supplemental Material [81]. From the band structures and the  $Z_2$  index calculations, we find that the  $M'_2M''C_3O_2$  MXenes are nontrivial topological semimetals. The orbital characters of the bands near the Fermi energy around the  $\Gamma$  point are very similar to those in the  $M'_2M''C_2O_2$  systems. Because of the local  $D_{3d}$  hexagonal symmetry, the touching valence and conduction bands at the  $\Gamma$  point are mainly dominated by  $d_{xy}$  and  $d_{x^2-y^2}$  orbitals of  $M'$  and  $M''$ . In  $Mo_2Hf_2C_3O_2$  and  $W_2Hf_2C_3O_2$ , the band inversion is induced by the SOC at the  $\Gamma$  point between W  $d_{xy}/d_{x^2-y^2}$  and W  $d_{3z^2-r^2}$  bands, while in the other  $M'_2M''C_3O_2$  ( $M' = Mo, W; M'' = Ti, Zr$ ) MXenes, the SOC only induces the band gap at the  $\Gamma$  point but the band inversion occurs due to the hybridization of the neighboring orbitals, similar to the  $M'_2M''C_2O_2$  systems.

#### IV. CONCLUSION

Here, we have searched for new topological insulators in recently synthesized double transition metal carbide MXenes, and found that  $M'_2M''C_2O_2$  ( $M' = Mo, W; M'' = Ti, Zr, Hf$ ) are topological insulators with the largest band gap of 0.285 eV (0.401 eV within the hybrid functional) for  $W_2HfC_2O_2$ . The large band gap, resulting from the strong SOC in transition metals  $M'$  and  $M''$ , is an attractive feature in these newly proposed topological insulators since the experimental realization of these systems with large band gaps would pave the way for practical applications of topological insulators at room temperature. In addition, we have found that  $M'_2M''C_3O_2$  with four transition metal layers are topological semimetals. Owing to various compositional and surface functional possibility, as well as thickness control, we expect more topological insulators and topological semimetals can be found in the

MXene family.

## ACKNOWLEDGMENTS

We gratefully thank Dr. Yan Sun for his fruitful discussions and helpful comments and analyses. The calculations were

performed on Numerical Materials Simulator at National Institute for Materials Science and RIKEN supercomputer system (HOKUSAI GreatWave).

- 
- [1] M. Z. Hasan and C. L. Kane, Colloquium: Topological insulators, *Rev. Mod. Phys.* **82**, 3045 (2010).
- [2] X. -L. Qi and S. -C. Zhang, Topological insulators and superconductors, *Rev. Mod. Phys.* **83**, 1057 (2011).
- [3] B. Yan and S.-C. Zhang, Topological materials, *Rep. Prog. Phys.* **75**, 096501 (2012).
- [4] H. Weng, R. Yu, X. Hu, X. Dai, and Z. Fang, Quantum anomalous Hall effect and related topological electronic states, *Adv. Phys.* **64**, 227 (2015).
- [5] B. A. Bernevig, T. L. Hughes, S. -C. Zhang, Quantum spin Hall effect and topological phase transition in HgTe quantum wells, *Science* **314**, 1757 (2006).
- [6] D. Hsieh, Y. Xia, D. Qian, L. Wray, J. H. Dil, F. Meier, J. Osterwalder, L. Patthey, J. G. Checkelsky, N. P. Ong, A. V. Fedorov, H. Lin, A. Bansil, D. Grauer, Y. S. Hor, R. J. Cava, and M. Z. Hasan, A tunable topological insulator in the spin helical Dirac transport regime, *Nature* **460**, 1101 (2009).
- [7] Y. L. Chen, J. G. Analytis, J.-H. Chu, Z. K. Liu, S.-K. Mo, X. L. Qi, H. J. Zhang, D. H. Lu, X. Dai, Z. Fang, S. C. Zhang, I. R. Fisher, Z. Hussain, and Z.-X. Shen, Experimental Realization of a Three-Dimensional Topological Insulator, Bi<sub>2</sub>Te<sub>3</sub>, *Science* **325**, 5937 (2009).
- [8] H. Zhang, C.-X. Liu, X.-L. Qi, X. Dai, Z. Fang, and S. C. Zhang, Topological insulators in Bi<sub>2</sub>Se<sub>3</sub>, Bi<sub>2</sub>Te<sub>3</sub> and Sb<sub>2</sub>Te<sub>3</sub> with a single Dirac cone on the surface, *Nat. Phys.* **5**, 438 (2009).
- [9] H. Lin, L. A. Wray, Y. Xia, S. Xu, S. Jia, R. J. Cava, A. Bansil, M. Z. Hasan, Half-Heusler ternary compounds as new multifunctional experimental platforms for topological quantum phenomena, *Nature* **9**, 546 (2010).
- [10] S. Chadov, X. Qi, J. Kübler, G.-H. Fecher, C. Felser, and S. -C. Zhang, Tunable multifunctional topological insulators in ternary Heusler compounds, *Nat. Mater.* **9**, 541 (2010).
- [11] H. Zhang and S.-C. Zhang, Topological insulators from the perspective of first-principles calculations, *Phys. Status Solidi RRL* **7**, 72 (2012).
- [12] L. Müchler, F. Casper, B. Yan, S. Chadov, and C. Felser, Topological insulators and thermoelectric materials, *Phys. Status Solidi RPL* **7**, 91 (2013).
- [13] L. Müchler, H. Zhang, S. Cadov, B. Yan, F. Casper, J. Kubler, S.-C. Zhang, and C. Felser, Topological Insulators from a chemist's perspective, *Angew. Chem. Int. Ed.* **51**, 7221 (2012).
- [14] J. Liu, T. G. Hesieh, P. Wei, W. Duan, J. Moodera, and L. Fu, Spin-filtered edge states with an electrically tunable gap in a two-dimensional topological crystalline insulator, *Nat. Mater.* **13**, 178 (2014).
- [15] Y. Sun, C. Felser, and B. Yan, Graphene-like Dirac states and quantum spin Hall insulators in square-octagonal MX<sub>2</sub> (M = Mo, W; X=S, Se, Te) isomers, *Phys. Rev. B* **92**, 165421, 2015.
- [16] L. Zhou, L. Kou, Y. Sun, C. Felser, F. Hu, G. Shan, S. C. Smith, B. Yan, and T. Frauenheim, New family of quantum spin Hall insulators in two-dimensional transition-metal halide with large nontrivial Band Gaps, *Nano Lett.* **15**, 7867 (2015).
- [17] P. Tang, P. Chen, W. Cao, H. Huang, S. Cahangirov, L. Xian, Y. Xu, S. -C. Zhang, W. Duan, and A. Rubio, Stable two-dimensional dumbbell stanene: A quantum spin Hall insulator, *Phys. Rev. B* **90**, 121408 (2014).
- [18] B. Yan, L. Müchler, and C. Felser, Prediction of weak topological insulators in layered semiconductors, *Phys. Rev. Lett.* **109**, 116406 (2012).
- [19] Y. Ma, Y. Dai, L. Kou, T. Frauenheim, and T. Heine, Robust two-dimensional topological insulators in methyl-functionalized bismuth, antimony, and lead bilayer films, *Nano Lett.* **15**, 1083 (2015).
- [20] F. -C. Chuang, L. -Z. Yao, Z. -Q. Huang, Y. -T. Liu, C. -H. Hsu, T. Das, H. Lin, and A. Bansil, Prediction of large-gap two-dimensional topological insulators consisting of bilayers of group III elements with Bi, *Nano Lett.* **14**, 2505 (2014).
- [21] F. -C. Chuang, C. -H. Hsu, C. Y. Chen, Z. -Q. Huang, V. Ozolins, H. Lin, and A. Bansil, Tunable topological electronic structures in Sb(111) bilayers: a first-principles study, *Appl. Phys. Lett.* **102**, 022424 (2013).
- [22] Y. Xu, B. Yan, H. -J. Zhang, J. Wang, G. Xu, P. Tang, W. Duan, and S. -C. Zhang, Large-gap quantum spin Hall insulators in thin films, *Phys. Rev. Lett.* **111**, 136804 (2013).
- [23] Y. Ma, L. Kou, Y. Dai, T. Heine, Discovery of a two-dimensional topological insulator in SiTe, *arXiv:1605.09654 [cond-mat.mtrl-sci]*.
- [24] A. Pham, C. J. Gil, S. C. Smith, and S. Li, Orbital engineering of two-dimensional materials with hydrogenation: a realization of giant gap and strongly correlated topological insulators, *Phys. Rev. B* **92**, 035427 (2015).
- [25] Y. Ma, L. Kou, X. Li, Y. Dai, S. C. Smith, and T. Heine, Quantum spin Hall effect and topological phase transition in two-dimensional square transition-metal dichalcogenides, *Phys. Rev. B* **92**, 085427 (2015).
- [26] M. Yang and W. -M. Liu, The d-p band-inversion topological insulator in bismuth-based skutterudites, *Scientific Reports* **4**, 5131 (2014).
- [27] P. -F. Liu, L. Zhou, T. Frauenheim, and L. -M. Wu, New quantum spin Hall insulator in two-dimensional MoS<sub>2</sub> with periodically distributed pores, *Nanoscale* **8**, 4915 (2016).
- [28] A. Wang, A. Du, and M. Zhao, Prediction of a large-gap quantum-spin-Hall insulator: diamond-like GaBi bilayer, *Nano Res.* **8**, 3823 (2015).
- [29] J. Zhao, Y. Li, and J. Ma, Quantum spin Hall insulators in functionalized arsenene (AsX, X = F, OH, and CH<sub>3</sub>) monolayers with pronounced light absorption, *Nanoscale* **8**, 9657 (2016).
- [30] B. -H. Chou, Z. -Q. Huang, C. -H. Hsu, F. -C. Chuang, Y. -T. Liu, H. Lin, and A. Bansil, Hydrogenated ultra-thin tin films predicted as two-dimensional topological insulators, *New J. Phys.* **16**, 115008 (2014).
- [31] L. Kou, F. Hu, B. Yan, T. Wehling, C. Felser, T. Frauenheim, C. Chen, Proximity enhanced quantum spin Hall state in graphene,

- Carbon* **87**, 418 (2015).
- [32] L. Kou, Y. Ma, B. Yan, X. Tan, C. Chen, and S. C. Smith, Encapsulated silicene: a robust large-gap topological insulator, *ACS Appl. Mater. Interfaces* **7**, 19226 (2015).
- [33] H. Zhang, Y. Ma, and Z. Chen, Quantum spin hall insulators in strain-modified arsenene, *Nanoscale* **7**, 19152 (2015).
- [34] Z. Song, C. -C. Liu, J. Yang, J. Han, M. Ye, B. Fu, Y. Yang, Q. Niu, J. Lu, and Y. Yao, Quantum spin Hall insulators and quantum valley Hall insulators of BiX/SbX (X = H, F, Cl and Br) monolayers with a record bulk band gap, *NPG Asia Mater.* **6**, e147 (2014).
- [35] Z. F. Wang, N. Su, F. Liu, Prediction of a two-dimensional organic topological insulator, *Nano Lett.* **13**, 2842 (2013).
- [36] A. Wang, X. Zhang, M. Zhao, Topological insulator states in honeycomb lattice of s-triazines, *Nanoscale* **7**, 11157 (2014).
- [37] C. Si, J. Liu, Y. Xu, J. Wu, B. -L. Gu, and W. Duan, Functionalized germanene as a prototype of large-gap two-dimensional topological insulators, *Phys. Rev. B* **89**, 115429 (2014).
- [38] H. -J. Sung, D. -H. Choe, and K. J. Chang, Tuning Dirac points by strain in MoX<sub>2</sub> nanoribbons (X = S, Se, Te) with a 1T' structure, *Phys. Chem. Chem Phys.* **18**, 16361 (2016).
- [39] H. Zhang, Ultrathin two-dimensional nanomaterials, *ACS Nano* **9**, 9451 (2015).
- [40] M. Naguib, M. Kurtoglu, V. Presser, J. Lu, J. Niu, M. Heon, L. Hultman, Y. Gogotsi, and M. W. Barsoum, Two-dimensional nanocrystals produced by exfoliation of Ti<sub>3</sub>AlC<sub>2</sub>, *Adv. Mater.* **23**, 4248 (2011).
- [41] M. Naguib, O. Mashtalir, J. Carle, V. Presser, J. Lu, L. Hultman, Y. Gogotsi, and M. W. Barsoum, Two-dimensional transition metal carbides, *ACS Nano* **6**, 1322 (2012).
- [42] M. Khazaei, M. Arai, T. Sasaki, M. Estili, and Y. Sakka, Trends in electronic structures and structural properties of MAX phases: a first-principles study on M<sub>2</sub>AlC (M = Sc, Ti, Cr, Zr, Nb, Mo, Hf, or Ta), M<sub>2</sub>AlN, and hypothetical M<sub>2</sub>AlB phases, *J. Phys.: Condens. Matter* **26**, 505503 (2014).
- [43] M. Khazaei, M. Arai, T. Sasaki, M. Estili, and Y. Sakka, The effect of the interlayer element on the exfoliation of layered Mo<sub>2</sub>AC (A=Al, Si, P, Ga, Ge, As or In) MAX phases into two-dimensional Mo<sub>2</sub>C nanosheets, *Sci. Tech. Adv. Mater.* **15**, 014208 (2014).
- [44] M. A. Hope, A. C. Forse, K. J. Griffith, M. Lukatskaya, M. Chidiu, Y. Gogotsi, and C. P. Grey, NMR reveals the surface functionalization of Ti<sub>3</sub>C<sub>2</sub> MXene, *Phys. Chem. Chem. Phys.* **18**, 5099 (2016).
- [45] K. J. Harris, M. Bugnet, M. Naguib, M. W. Barsoum, and G. R. Goward, Direct measurement of surface termination groups and their connectivity in the 2D MXene V<sub>2</sub>CT<sub>x</sub> using NMR spectroscopy, *J. Phys. Chem. C* **119**, 13713 (2015).
- [46] R. Meshkini, L. -Å. Näsiund, J. Halim, Synthesis of two-dimensional molybdenum carbide, Mo<sub>2</sub>C, from the gallium based atomic laminate Mo<sub>2</sub>Ga<sub>2</sub>C, *Scr. Mater.* **108**, 147 (2015).
- [47] J. Yang, M. Naguib, M. Ghidiu, L. -M. Pan, J. Gu, J. Nanda, J. Halim, Y. Gogotsi, M. W. Barsoum, Two-dimensional Nb-based M<sub>4</sub>C<sub>3</sub> solid solutions (MXenes), *J. Am. Ceramic Soc.* **99**, 660 (2016).
- [48] M. Khazaei, M. Arai, T. Sasaki, C. -Y. Chung, N. S. Venkataramanan, M. Estili, Y. Sakka, and Y. Kawazoe, Novel electronic and magnetic properties of two-dimensional transition metal carbides and nitrides, *Adv. Funct. Mater.* **23**, 2185 (2013).
- [49] M. Khazaei, A. Ranjbar, M. Ghorbani-Asl, M. Arai, T. Sasaki, Y. Liang, and S. Yunoki, Nearly free electron states in MXenes, *Phys. Rev. B* **93**, 205125 (2016).
- [50] M. Khazaei, M. Arai, T. Sasaki, M. Estili, and Y. Sakka, Two-dimensional molybdenum carbides: potential thermoelectric materials of the MXene family, *Phys. Chem. Chem. Phys.* **16**, 7841 (2014).
- [51] M. Khazaei, M. Arai, T. Sasaki, A. Ranjbar, Y. Liang, and S. Yunoki, OH-terminated two-dimensional transition metal carbides and nitrides as ultralow work function materials, *Phys. Rev. B* **92**, 075411 (2015).
- [52] C. Si, J. Zhou, and Z. Sun, Half-metallic ferromagnetism and surface functionalization-induced metal-insulator transition in graphene-like two-dimensional Cr<sub>2</sub>C crystals, *ACS Appl. Mater. Interfaces* **7**, 17510 (2015).
- [53] Y. Bai, K. Zhou, N. Srikanth, J. H. L. Pang, X. He, and R. Wang, Dependence of elastic and optical properties on surface terminated groups in two-dimensional MXene monolayers: a first-principles study, *RSC Adv.* **6**, 35731 (2016).
- [54] C. Ling, L. Shi, Y. Ouyang, Q. Chen, and J. Wang, Transition metal-promoted V<sub>2</sub>CO<sub>2</sub> (MXenes): a new and highly active catalyst for hydrogen evolution reaction, *Adv. Sci.* (2016), DOI:10.1002/advs.201600180.
- [55] J. Yang, X. Luo, S. Zhang, and L. Chen, Investigation of magnetic and electronic properties of transition metal doped Sc<sub>2</sub>CT<sub>2</sub> (T = O, OH or F) using a first principles study, *Phys. Chem. Chem. Phys.* **18**, 12914 (2016).
- [56] L. Hong, R. F. Klie, and S. Ögüt, First-principles study of size- and edge-dependent properties of MXene nanoribbons, *Phys. Rev. B* **93**, 115412 (2016).
- [57] X. -H. Zha, J. Zhou, Y. Zhou, Q. Huang, J. He, J. S. Francisco, Kan Luo, and Shiyu Du, Promising electron mobility and high thermal conductivity in Sc<sub>2</sub>CT<sub>2</sub> (T = F, OH) MXenes, *Nanoscale* **8**, 6110 (2016).
- [58] J. He, P. Lyu, L. Z. Sun, Á. M. García, and P. Nachtigall, High temperature spin-polarized semiconductivity with zero magnetization in two-dimensional Janus MXenes, *J. Mater. Chem. C* **4**, 6500 (2016).
- [59] G. Gao, G. Ding, J. Li, K. Yao, M. Wu, and M. Qian, Monolayer MXenes: promising half-metals and spin gapless semiconductors, *Nanoscale* **8**, 8986 (2016).
- [60] Y. Xie, Y. Dall'Agnese, M. Naguib, Y. Gogotsi, M. W. Barsoum, H. L. Zhuang, and P. R. C. Kent, Prediction and characterization of MXene nanosheet anodes for non-lithium-ion batteries, *ACS Nano* **8**, 9606 (2014).
- [61] U. Yorulmaz, A. Özden, N. K. Perkgöz, F. Ay, and C. Sevik, Vibrational and mechanical properties of single layer MXene structures: a first-principles investigation, *Nanotechnology* **27**, 335702 (2016).
- [62] X. -H. Zha, J. Yin, Y. Zhou, Q. Huang, K. Luo, J. Lang, J. S. Francisco, J. He, and S. Du, Intrinsic structural, electrical, thermal, and mechanical properties of the promising conductor Mo<sub>2</sub>C MXene, *J. Phys. Chem. C* **120**, 15082 (2016).
- [63] H. Fashandi, V. Ivády, P. Eklund, A. L. Spetz, M. I. Katsnelson, and I. A. Abrikosov, Dirac points with giant spin-orbit splitting in the electronic structure of two-dimensional transition metal carbides, *Phys. Rev. B* **92**, 155142 (2015).
- [64] H. Weng, A. Ranjbar, Y. Liang, Z. Song, M. Khazaei, S. Yunoki, M. Arai, Y. Kawazoe, Z. Fang, and X. Dai, Large-gap two-dimensional topological insulator in oxygen functionalized MXene, *Phys. Rev. B* **92**, 075436 (2015).
- [65] B. Anasori, Y. Xie, M. Beidaghi, J. Lu, B. C. Hosler, L. Hultman, P. R. C. Kent, Y. Gogotsi, and M. W. Barsoum, Two-dimensional, ordered, double transition metals carbides (MXenes), *ACS Nano* **9**, 9507 (2016).
- [66] B. Anasori, C. Shi, E. J. Moon, Y. Xie, C. A. Voigt, P. R. C. Kent, S. J. May, S. J. L. Billinge, M. W. Barsoum, and Y. Gogotsi, Control of electronic properties of 2D carbides (MXenes) by manipulating their transition metal layers,

- Nanoscale Horiz.* **1**, 227 (2016).
- [67] B. Anasori, M. Dahlqvist, J. Halim, E. J. Moon, J. Lu, B. C. Hosler, E. N. Caspi, S. J. May, L. Hultman, P. Eklund, J. Rosén and M. W. Barsoum, Experimental and theoretical characterization of ordered MAX phases  $\text{Mo}_2\text{TiAlC}_2$  and  $\text{Mo}_2\text{Ti}_2\text{AlC}_3$ , *J. Appl. Phys.* **118**, 094304 (2015).
- [68] O. Mashtalir, M. Naguib, V. N. Mochalin, Y. Dall'Agnesse, M. Heon, M. W. Barsoum, and Y. Gogotsi, Intercalation and delamination of layered carbides and carbonitrides, *Nat. Commun.* **4**, 1716 (2013).
- [69] M. R. Lukatskaya, O. Mashtalir, C. E. Ren, Y. Dall'Agnesse, P. Rozier, P. L. Taberna, M. Naguib, P. Simon, M. W. Barsoum, and Y. Gogotsi, Cation intercalation and high volumetric capacitance of two-dimensional titanium carbide, *Science* **341**, 1502 (2013).
- [70] G. Kresse and J. Furthmüller, Efficiency of ab-initio total energy calculations for metals and semiconductors using a plane-wave basis set, *Comput. Mater. Sci.* **6**, 15 (1996).
- [71] J. P. Perdew, K. Burke, and M. Ernzerhof, Generalized gradient approximation made simple, *Phys. Rev. Lett.* **77**, 3865 (1996).
- [72] H. J. Monkhorst and J. D. Pack, Special points for Brillouin-zone integrations, *Phys. Rev. B* **13**, 5188 (1976).
- [73] J. Heyd, G. E. Scuseria, and M. Ernzerhof, Hybrid functionals based on a screened coulomb potential, *J. Chem. Phys.* **118**, 8207 (2003).
- [74] J. Heyd, G. E. Scuseria, and M. Ernzerhof, Erratum: Hybrid functionals based on a screened Coulomb potential [*J. Chem. Phys.* **118**, 8207 (2003)], *J. Chem. Phys.* **124**, 219906(E) (2006).
- [75] S. Baroni, S. de Gironcoli, A. Dal. Corso, and P. Gianozzi, Phonons and related crystal properties from density-functional perturbation theory, *Rev. Mod. Phys.* **73**, 515 (2001).
- [76] P. Giannozzi *et al.*, QUANTUM ESPRESSO: a modular and open-source software project for quantum simulations of materials, *J. Phys.: Condens. Matter* **21**, 395502 (2009).
- [77] N. Marzari and D. Vanderbilt, Maximally localized generalized Wannier functions for composite energy bands, *Phys. Rev. B* **56**, 12847 (1997).
- [78] I. Souza, N. Marzari, and D. Vanderbilt, Maximally localized Wannier functions for entangled energy bands, *Phys. Rev. B* **65**, 035109 (2001).
- [79] <http://www.openmx-square.org>.
- [80] M. Ashton, K. Mathew, R. G. Hennig, and S. B. Sinnott, Predicted surface composition and thermodynamic stability of MXenes in solution, *J. Phys. Chem. C* **120**, 3550 (2016).
- [81] See Supplemental Material at <http://link.aps.org/supplemental/10.1103/> for the predicted structures, the band structures using VASP and Quantum Espresso.
- [82] X. Zhang, X. -F. Qiao, W. Shi, J. -B. Wu, D. -S. Jiang, and P. -H. Tan, Phonon and Raman scattering of two-dimensional transition metal dichalcogenides from monolayer, multilayer to bulk material, *Chem. Soc. Rev.* **44**, 2757 (2015).
- [83] D. L. Mafra and P. T. Araujo, Intra- and interlayer electron-phonon interactions in  $^{12/13}\text{C}$  and  $^{12/13}\text{C}$  bilayer graphene, *Appl. Sci.* **4**, 207 (2014).
- [84] L. Fu, C. L. Kane, and E. J. Mele, Topological insulators in three dimensions, *Phys. Rev. Lett.* **98**, 106803 (2007).
- [85] L. Fu and C. L. Kane, Topological insulators with inversion symmetry, *Phys. Rev. B* **76**, 045302 (2007).
- [86] H. Weng, X. Dai, and Z. Fang, Transition-Metal Pentatelluride  $\text{ZrTe}_5$  and  $\text{HfTe}_5$ : A Paradigm for Large-Gap Quantum Spin Hall Insulators, *Phys. Rev. X* **4**, 011002 (2014).